Reactive Collision Avoidance for Underactuated Surface Vehicles using the Collision Cone Concept

Aurora Haraldsen[1], Martin S. Wiig[2] and Kristin Y. Pettersen[1,2]

***Abstract*— Avoiding collisions is a crucial task for autonomous systems. Many strategies for avoiding obstacles have been proposed, yet the problem of having underactuated dynamics is rarely addressed in previous studies of collision avoidance algorithms. Underactuation of a system makes the collision avoidance control problem more complex, since the system then lacks the ability to directly control one or more of its degrees of freedom. Therefore, in this paper, we will consider collision avoidance for underactuated vehicles, specifically for the class of vehicles which cannot directly control their sideways speed. This is a broad class, which includes vehicles such as cars, airplanes, and marine vehicles. If the unactuated, sideways velocity component becomes sufficiently large, it can make the vehicle glide sideways rather than moving forward, which in the encounter with an obstacle may be fatal. To tackle this issue, we propose a reactive collision avoidance algorithm, based on the collision cone concept, which is specifically designed to account for the underactuated dynamics of a surface vehicle. We present a rigorous analysis of the closed-loop system and establish explicit conditions guaranteeing vehicle safety. Simulations are included to verify the theoretical result.**

***Index Terms*— collision avoidance, marine vehicles, underactuated systems, real-time control, nonlinear dynamical systems**

I. Introduction

Autonomous and unmanned vehicles present a large potential for both scientific and commercial applications. They are already employed in several areas, such as subsea inspection and intervention, surveillance, transportation, and space operations. The vehicles are required to navigate in complex, dynamic environments while performing autonomous or semi-autonomous operations. Collision avoidance (CA) of obstacles is a critical part of the navigation due to the severe consequences of a failure. CA algorithms are often divided in two groups: reactive algorithms and motion planning algorithms. The latter group generally depends on planning, and often rely on optimization methods. This can be time-consuming for vehicles with complex dynamics, navigating in dense environments. Optimization problems can furthermore become computationally intractable for large and complex search spaces. Hence, autonomous vehicles must generally rely on backup solutions that are computationally simpler and yet provably safe, i.e. reactive algorithms.

Reactive algorithms compute only one next action at each instant and therefore cope well with highly dynamic and unpredictable environments. A well-established approach for reactive collision avoidance is the velocity obstacle (VO) algorithm [1]. The method is based on describing obstacles in the velocity space by computing the set of relative velocities between the vehicle and an obstacle which result in a future collision. By maintaining velocities outside of this set, the vehicle necessarily avoids a collision. This set is termed the collision cone. The VO algorithm is conceptually similar to the collision cone approach [2] which has developed necessary and sufficient conditions for collision with obstacles of arbitrary shape and time-varying velocities, based on the collision cone theory. Contrary to the VO method which evaluates obstacles in the velocity space, the collision cone approach is guidance based. The method has been used to construct guidance laws for both cooperative control [3] and general obstacle avoidance [4].

We have previously applied the collision cone concept to a nonholonomic vehicle [5], where we provide guarantees for avoidance of a dynamic, unpredictable obstacle. In this paper, we extend the method to incorporate the dynamics of a surface vehicle that is able to generate a forward thrust and a momentum in yaw, but lacks actuation in the sideways direction. Although the vehicle has no sideways actuation, forces in the sideways direction are generated when the vehicle turns whilst moving forward, due to the centripetal and to some extent the Coriolis effects. As the motion of the vehicle depends on both the sideways and forward velocity, the unactuated velocity component will significantly affect its maneuvers. The underactuated dynamics must therefore be properly accounted for in order to ensure safety.

Although the VO method and the collision cone approach have been applied to different dynamical systems, e.g. [6], [3], [7], [8], [9], hardly any analyze the resulting closed-loop system dynamics, much less the underactuated dynamics. The main contribution of this paper is therefore the establishment and analysis of a collision avoidance law which provably ensures that an underactuated surface vehicle avoids a collision with a dynamic, uncooperative obstacle that is able to change both speed and direction at any instant, under explicitly stated conditions. Similar to the constant avoidance angle (CAA) algorithm [10] which has been applied to underactuated marine vehicles, the proposed method steers the vehicle a constant angle to the side of the obstacle. In the CAA algorithm, the angle is chosen to make the vehicle circumvent an obstacle at a constant distance and therefore differs from collision cone approaches in that it does not require knowledge of the obstacle shape. In the proposed approach, the angle comprises an additional safety measure, chosen specifically to account for the fact that the

[1]Centre for Autonomous Marine Operations and Systems (NTNU AMOS), Department of Engineering Cybernetics, Norwegian University of Science and Technology, NO-7491 Trondheim, Norway.

[2]Norwegian Defence Research Establishment (FFI), P.O. Box 25, N-2027 Kjeller, Norway.

Dette er en postprint-versjon/This is a postprint version.
DOI til publisert versjon/DOI to published version: 10.1109/CCTA48906.2021.9659043

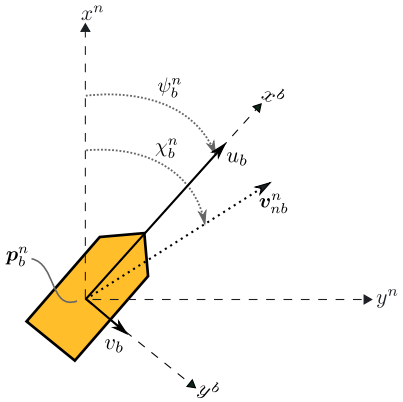

Fig. 1: The body-fixed reference frame in relation to the inertial reference frame.

vehicle cannot change its yaw rate momentarily. Another similarity to the CAA algorithm is that we choose to control the course of the vehicle rather than its heading, which ensures that the vehicle is steered in the desired direction. In [10], proportional-derivative control of the course is applied, and safe course references are assigned to make the vehicle avoid potential collisions. Although this control solution stabilizes the course error dynamics exponentially, it does not utilize the turning capabilities of the vehicle to the fullest in collision avoidance scenarios. In our approach, we instead let the vehicle turn at a constant, maximum rate to avoid collision, thus generating faster and more agile avoidance maneuvers. The collision avoidance problem is moreover combined with path following to demonstrate that the approach also allows the vehicle to achieve its separate goals.

The paper is organized as follows. Section II and III present the vehicle and obstacle models, respectively, and Section IV defines the geometrical properties of the collision cone. In Section V the control system of the vehicle is presented. A mathematical analysis of the algorithm applied to the system is given in Section VI. The theoretical results are verified through simulations in Section VII, before some concluding remarks are provided in Section VIII.

II. Vehicle model

We will in this section explain the notation used to express the vehicle kinematics and present the kinematic and dynamic model of an underactuated surface vehicle.

A. Notation

The vehicle is modeled in three degrees of freedom. The model is expressed in the body frame b, which is attached to the pivot point [11] of the vehicle, in reference to an inertial frame n (cf. Figure 1). The position and velocity of b with respect to n are denoted as $\boldsymbol{p}_b^n \triangleq [x_b^n,\, y_b^n]^\top$ and $\boldsymbol{v}_{nb}^n \triangleq [\dot{x}_b^n,\, \dot{y}_b^n]^\top$, respectively, and the orientation of b with respect to n is given by the heading angle ψ_b^n. The body-fixed linear and angular velocities are contained in the vector $\boldsymbol{\nu}_{nb}^b \triangleq [u_b,\, v_b,\, r_b]^\top$, where u_b is the surge (forward) speed, v_b is the sway (sideways) speed, and r_b is the yaw (heading) rate. The speed of the vehicle is denoted as $U_b \triangleq \sqrt{u_b^2 + v_b^2}$ and the course as $\chi_b^n \triangleq \operatorname{atan2}(\dot{y}_b^n, \dot{x}_b^n)$.

B. Model

The marine vehicle is assumed to have a thruster generating force in the forward direction and a rudder generating angular momentum. The model is written in the expanded form of [10]:

$$\dot{x}_b^n = u_b \cos(\psi_b^n) - v_b \sin(\psi_b^n), \tag{1a}$$
$$\dot{y}_b^n = u_b \sin(\psi_b^n) + v_b \cos(\psi_b^n), \tag{1b}$$
$$\dot{\psi}_b^n = r_b, \tag{1c}$$
$$\dot{u}_b = f_u(u_b, v_b, r_b) + \tau_u, \tag{1d}$$
$$\dot{v}_b = X(u_b) r_b + Y(u_b) v_b, \tag{1e}$$
$$\dot{r}_b = f_r(u_b, v_b, r_b) + \tau_r, \tag{1f}$$

where the expressions of $f_u(u_b, v_b, r_b)$, $f_r(u_b, v_b, r_b)$, $X(u_b)$, and $Y(u_b)$ depend on the mass and damping coefficients of the vehicle and are given in Appendix A, and τ_u and τ_r are the control forces in surge and yaw, respectively. For the full derivation of the model (1) we refer you to [10], as well as [12] on modeling of marine vehicles in general.

Remark 1. The model (1) is valid for surface vehicles, and also for describing the horizontal motion of underwater vehicles, operating at maneuvering speeds.

III. Obstacle model

The obstacle is modeled as a moving, circular domain $\mathcal{D}_o$, with a radius of R_o, described by the kinematic equations:

$$\dot{x}_o^n = u_o \cos(\psi_o^n), \tag{2a}$$
$$\dot{y}_o^n = u_o \sin(\psi_o^n), \tag{2b}$$
$$\dot{\psi}_o^n = r_o, \tag{2c}$$
$$\dot{u}_o = a_o, \tag{2d}$$

where x_o^n and y_o^n are the Cartesian coordinates of the obstacle center, u_o and a_o are the forward speed and acceleration, and ψ_o^n and r_o are the obstacle heading and heading rate, respectively. The position of the obstacle center is denoted as $\boldsymbol{p}_o^n \triangleq [x_o^n, y_o^n]^\top$ and the velocity as $\boldsymbol{v}_{no}^n \triangleq [\dot{x}_o^n, \dot{y}_o^n]^\top$.

Assumption 1. The heading rate, r_o, and forward acceleration, a_o, are bounded by

$$r_o \in [-r_{o,\max},\, r_{o,\max}], \tag{3}$$
$$a_o \in [-a_{o,\max},\, a_{o,\max}], \tag{4}$$

where $r_{o,\max} \geq 0$ and $a_{o,\max} \geq 0$ are constant parameters.

Assumption 2. The forward speed, u_o, is bounded by

$$u_o \in [0,\, u_{o,\max}], \tag{5}$$

where $u_{o,\max} < u_b$ is a constant parameter.

Remark 2. By Assumption 2, we require the forward speed of the vehicle, u_b, to be lower bounded by the maximum forward speed of the obstacle. This ensures well-definedness of the geometrical properties defined in the following section and is generally a necessary assumption for guaranteeing avoidance of a dynamic, uncooperative obstacle.

Dette er en postprint-versjon/This is a postprint version.
DOI til publisert versjon/DOI to published version: 10.1109/CCTA48906.2021.9659043

IV. The collision cone

To keep the vehicle away from collision, the proposed algorithm will make the vehicle maintain a course that avoids a collision with the obstacle by the collision cone notion. To remain out of collision, the vehicle should keep at least a distance $d_{\text{sep}} > R_o$ to the obstacle center.

Definition 1 (Collision)**.** A collision occurs between the vehicle and the obstacle if

$$d_{b,o} < d_{\text{sep}}, \tag{6}$$

where $d_{b,o} \triangleq \|\boldsymbol{p}_b^n - \boldsymbol{p}_o^n\|$.

Consider a coordinate frame n_o, aligned with the inertial frame n, moving with the obstacle velocity, $\boldsymbol{v}_{no}^n$. In this frame, the obstacle is static and the vehicle has the velocity $\boldsymbol{v}_{nbo}^n \triangleq \boldsymbol{v}_{nb}^n - \boldsymbol{v}_{no}^n$ and course $\chi_{bo}^n \triangleq \text{atan2}(\dot{y}_b^n - \dot{y}_o^n,\, \dot{x}_b^n - \dot{x}_o^n)$. The vehicle is in danger of colliding with the obstacle if its course, given in n_o, lies between the angles

$$\psi_{\text{cc}}^{\pm} \triangleq \alpha \pm \beta, \tag{7}$$

where we use the superscript $\pm$ to distinguish between the two angles, representing the edges of the collision cone. Moreover, $\alpha \triangleq \text{atan2}\left(y_o^n - y_b^n,\, x_o^n - x_b^n\right)$ and

$$\beta \triangleq \arcsin\left(\frac{d_{\text{sep}}}{d_{b,o}}\right), \tag{8}$$

as shown in Figure 2a. Motivated by [13], we will call this situation a *conflict*, which is characterized by the condition

$$|\chi_{bo}^n - \alpha| < \beta. \tag{9}$$

The same condition can be described with respect to the inertial frame, n, by performing a coordinate transformation. Consider Figure 2b, where we let the velocity vector $\boldsymbol{v}_{nbo}^n$ point along the edge at ψ_{cc}^+. The angle χ_{cc}^+ then defines the corresponding edge given in n, computed as

$$\chi_{\text{cc}}^{\pm} \triangleq \psi_{\text{cc}}^{\pm} + \gamma_b^{\pm}. \tag{10}$$

Remark 3. The angle χ_{cc}^- is computed by the same procedure as χ_{cc}^+.

The angle γ_b^+ can be found by using the Law of Sines on the triangle defined by $\boldsymbol{v}_{nb}^n$, $-\boldsymbol{v}_{no}^n$, and $\boldsymbol{v}_{nbo}^n$, as

$$\gamma_b^{\pm} \triangleq \arcsin\left(\frac{u_o \sin\left(\gamma_o^{\pm}\right)}{U_b}\right), \tag{11}$$

where γ_o^+ is found geometrically as

$$\gamma_o^{\pm} \triangleq \pi - \psi_o^n + \psi_{\text{cc}}^{\pm}. \tag{12}$$

Adapted from [13], a measure of the angular distances to a conflict with the obstacle is then found as

$$\delta^{\pm} \triangleq \pm\chi_b^n \mp \chi_{\text{cc}}^{\pm}. \tag{13}$$

The angles are wrapped into the domain $\delta^{\pm} \in (-2\pi,\, 2\pi]$ such that they are negative if the vehicle is in a conflict, and positive otherwise. The formulation corresponds to the distances the vehicle must turn in both directions in order to enter (or in the opposite case, exit) a conflict, and the shortest distance is found geometrically as

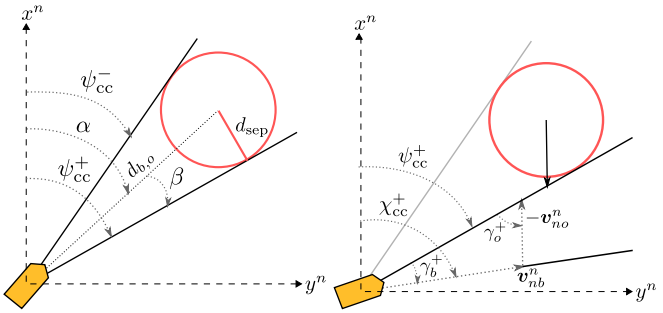

(a) Representation of $\psi_{\text{cc}}^{\pm}$. (b) Decomposition of χ_{cc}^+.

Fig. 2: Geometric representation of the collision cone.

$$\delta^{\min} \triangleq \begin{cases} \delta^+ & \text{if } \chi_{bo}^n - \alpha \geq 0, \\ \delta^- & \text{if } \chi_{bo}^n - \alpha < 0, \end{cases} \tag{14}$$

where we map the angular difference to the interval $(\chi_{bo}^n - \alpha) \in (-\pi,\, \pi]$.

V. Vehicle control

This section presents the full control system of the vehicle. The objective of the vehicle is to converge to a straight-line path by following the course references generated by a line-of-sight (LOS) guidance law. To ensure that path following does not lead to a collision, the course of the vehicle is controlled by a collision avoidance algorithm at all times. Notice that, as opposed to vehicles with unicycle-like kinematics, the heading and the course of the vehicle (1) do not necessarily coincide. In particular, at non-zero sway speeds, the vehicle will move in a direction that differs from its heading. To circumvent this issue, the output of the course control law is converted to an equivalent yaw rate signal. The dynamics of the vehicle are moreover controlled by feedback linearizing controllers, ensuring close tracking of the surge speed and yaw rate references.

A. Path following

The objective of the vehicle is to follow a straight-line path parallel to the x^n-axis, defined as $\mathcal{P} \triangleq \{(x, y) \in \mathbb{R}^2 \mid y = y_{\text{t}}^n\}$, where y_{t}^n is the desired position along the y^n-axis. To make the vehicle converge to and move along this path, we choose to use an LOS guidance law [12] to define the desired course angle as

$$\chi_{\text{gd}}^n \triangleq \arctan\left(-\frac{y_b^n - y_{\text{t}}^n}{\Delta}\right), \tag{15}$$

where $\Delta > 0$ is the lookahead distance. To ensure that the vehicle maintains this course, the desired course rate is chosen as

$$r_{\text{gd}} \triangleq \dot{\chi}_{\text{gd}}^n - \lambda_\chi \tilde{\chi}_{\text{g}}^n, \tag{16}$$

where $\tilde{\chi}_{\text{g}}^n \triangleq \chi_b^n - \chi_{\text{gd}}^n$ and $\lambda_\chi > 0$ is a constant gain. It is straightforward to see that the control law (16) ensures global exponential stability of the course error dynamics, provided the desired course rate, r_{gd}, is perfectly tracked.

Dette er en postprint-versjon/This is a postprint version.
DOI til publisert versjon/DOI to published version: 10.1109/CCTA48906.2021.9659043

B. Collision avoidance

To avoid colliding into an obstacle, the vehicle should always abide by a collision avoidance algorithm. A safety radius $R_{\text{safe}} > 0$ is introduced to determine when collision avoidance is needed. If the obstacle is outside of this radius,

$$d_{b,o} > R_{\text{safe}}, \tag{17}$$

then the vehicle should always maintain path following. However, if the obstacle comes within the safety radius, path following should continue as long as the guidance law is safe to follow, determined by the condition:

$$\chi_{\text{gd}}^n \notin \mathcal{V}_{\text{cc}}^\epsilon \text{ and } d_{b,o} \geq \frac{d_{\text{sep}}}{\cos(\epsilon)}, \tag{18}$$

where $\mathcal{V}_{\text{cc}}^\epsilon \triangleq \left(\chi_{\text{cc}}^- - \epsilon,\, \chi_{\text{cc}}^+ + \epsilon\right)$ and $\epsilon \geq 0$ is a constant safety angle. If either of the safety conditions (17) and (18) holds, the desired course rate is thus chosen by (16). Otherwise, the desired course rate is chosen by a collision avoidance law, which will be presented shortly.

To avoid oscillations, the initial turning direction of the vehicle is held throughout the avoidance maneuver, chosen as

$$j_0 \triangleq \arg\min_{j \in \{\pm\}} \left| \delta^{(j)} \right|, \tag{19}$$

evaluated at the time the control system switches from path following to collision avoidance. In order to avoid a potential collision, the vehicle should maintain some maximum course rate, $r_{\chi,\max} > 0$, in the chosen direction until a safe course is obtained. The collision avoidance law is thus chosen as

$$r_{\text{ca}} \triangleq \begin{cases} \pm r_{\chi,\max} & \text{if } \delta^{\min} \leq 0 \mid j_0 = \pm, \\ \lambda_\delta \left(\pm\epsilon \mp \delta^{\min}\right) & \text{if } \delta^{\min} > 0 \mid \delta^{\min} = \delta^{\pm}, \end{cases} \tag{20}$$

where $\lambda_\delta > 0$ is a constant gain. The second case of (20) will make the vehicle maintain a safety angle, ϵ, to a conflict with obstacle and always coincides with the turning parameter j_0. This ensures that the vehicle does not diverge further than necessary from the nominal trajectory. Moreover, the safety angle acts as an additional security for the vehicle when the obstacle is at a close distance. We will provide lower bounds of the safety parameters ϵ and R_{safe} in Section VI.

C. Surge and yaw controllers

Let $u_{b\text{d}}$ and $r_{b\text{d}}$ denote the desired surge speed and yaw rate, respectively, where $u_{b\text{d}} > 0$ is constant and $r_{b\text{d}}$ will be defined in the next section. The surge and yaw dynamics are controlled by the feedback linearizing controllers:

$$\tau_u = \dot{u}_{b\text{d}} - f_u(u_b, v_b, r_b) - \lambda_u \tilde{u}_b, \tag{21a}$$

$$\tau_r = \dot{r}_{b\text{d}} - f_r(u_b, v_b, r_b) - \lambda_r \tilde{r}_b, \tag{21b}$$

where $\tilde{u}_b \triangleq u_b - u_{b\text{d}}$, $\lambda_u > 0$ is the surge control gain, $\tilde{r}_b \triangleq r_b - r_{b\text{d}}$, and $\lambda_r > 0$ is the yaw control gain. Substituting (21) into the dynamics (1) verifies that the surge and yaw error dynamics are linear and globally exponentially stable.

Assumption 3. At the time t_0, the system has operated long enough for the yaw rate and surge speed to converge, i.e. $\tilde{r}_b(t_0) = 0$ and $\tilde{u}_b(t_0) = 0$.

D. Course rate to yaw rate conversion

The course rate, defined as $r_\chi \triangleq \dot{\chi}_b^n$, is computed by differentiating $\chi_b^n \triangleq \psi_b^n + \arctan\left(\frac{v_b}{u_b}\right)$ with respect to time:

$$r_\chi = \frac{U_b^2 + X(u_b)u_b}{U_b^2} r_b + \frac{Y(u_b)u_b}{U_b^2} v_b, \tag{22}$$

where we have used the fact that $\dot{u}_b = 0$, ensured by Assumption 3. Thus, substituting $u_{b\text{d}}$ for u_b, the desired yaw rate is defined as

$$\bar{r}_{b\text{d}} \triangleq \frac{U_{b\text{d}}^2 r_{\chi\text{d}} - Y_{u\text{d}} u_{b\text{d}} v_b}{U_{b\text{d}}^2 + X_{u\text{d}} u_{b\text{d}}}, \tag{23}$$

where $r_{\chi\text{d}}$ denotes the desired course rate of the vehicle, chosen as either (16) or (20) by the collision avoidance algorithm, and the notation $U_{b\text{d}} \triangleq \sqrt{u_{b\text{d}}^2 + v_b^2}$, $X_{u\text{d}} \triangleq X(u_{b\text{d}})$, and $Y_{u\text{d}} \triangleq Y(u_{b\text{d}})$ is adopted for conciseness.

Assumption 4. The term $X(u_b)$ satisfies

$$X(u_b) + u_b > 0. \tag{24}$$

Remark 4. Assumption 4 implies that a change in the yaw of the vehicle results in a change in its course, which can be seen directly from (22). This is a valid assumption for marine vehicles and ensures that (23) is well-defined.

The modular structure of the algorithm will inevitably cause discontinuities in the reference signal (23). Let t_{d} denote a time at which such a jump occurs. To ensure that the reference is smooth and can thus be tracked immediately, we compute it as

$$r_{b\text{d}} \triangleq \begin{cases} r_{b\text{d}}\left(t_{\text{d}}\right) + \frac{T_{\text{d}}}{T_{\text{s}}}\left(\bar{r}_{b\text{d}}\left(t_{\text{d}}\right) - r_{b\text{d}}\left(t_{\text{d}}\right)\right) & \text{if } T_{\text{d}} < T_{\text{s}}, \\ \bar{r}_{b\text{d}} & \text{otherwise}, \end{cases} \tag{25}$$

where $T_{\text{s}} > 0$ is a smoothing interval and $T_{\text{d}} \triangleq t - t_{\text{d}}$. Note that the parameters t_{d} and T_{s} are updated in line with changes in $\bar{r}_{b\text{d}}$ to avoid overshoots.

VI. Mathematical analysis

This section presents an analysis of the closed-loop behavior of the underactuated vehicle and associated control system. We begin by establishing a lower bound of the distance the vehicle keeps to the obstacle in the ideal case.

Lemma 1. *Consider an obstacle moving with the time-varying velocity $\boldsymbol{v}_{no}^n$. Suppose that the vehicle satisfies*

$$|\chi_{bo}^n(t) - \alpha(t)| \geq \beta(t) + \epsilon, \;\; \forall t \geq t_0, \tag{26}$$

where $\epsilon \in \left[0, \frac{\pi}{2}\right)$ is a constant angle, and suppose that $d_{b,o}(t_0) \geq \frac{d_{\text{sep}}}{\cos(\epsilon)}$. Then,

$$d_{b,o}(t) \geq \frac{d_{\text{sep}}}{\cos(\epsilon)}, \;\; \forall t \geq t_0. \tag{27}$$

Proof: Consider the line segment going from the vehicle center, $\boldsymbol{p}_b^n$, to the obstacle center, $\boldsymbol{p}_o^n$, with length $d_{b,o}$ and orientation α. The time-derivative of $d_{b,o}$ is found geometrically as

$$\dot{d}_{b,o} = -U_{bo}\cos(\chi_{bo}^n - \alpha), \tag{28}$$

Dette er en postprint-versjon/This is a postprint version.
DOI til publisert versjon/DOI to published version: 10.1109/CCTA48906.2021.9659043

where $U_{bo} \triangleq \|\boldsymbol{v}_{nbo}^n\|$. Substituting (26) in (28) gives

$$\beta \leq \arccos\left(-\frac{\dot{d}_{b,o}}{U_{bo}}\right) - \epsilon, \tag{29}$$

and the time-derivative of β is computed from (8) as

$$\dot{\beta} = -\frac{\dot{d}_{b,o}}{d_{b,o}}\tan(\beta). \tag{30}$$

Moreover, the initial condition $d_{b,o}(t_0) \geq \frac{d_{\text{sep}}}{\cos(\epsilon)}$ entails that $\beta(t_0) \leq \frac{\pi}{2} - \epsilon$. Since $\dot{\beta} < 0, \forall \dot{d}_{b,o} > 0$ by (30) and $\beta \leq \frac{\pi}{2} - \epsilon, \forall \dot{d}_{b,o} \leq 0$ by (29), we have $\beta(t) \leq \frac{\pi}{2} - \epsilon, \forall t \geq t_0$. Solving (8) for the distance, $d_{b,o}$, with $\beta \leq \frac{\pi}{2} - \epsilon$, yields (27), which concludes the proof. ∎

For the next lemma, we require the sway dynamics (1e) to be nominally stable:

Assumption 5. The term $Y(u_b)$ satisfies

$$Y(u_b) < 0. \tag{31}$$

Due to the hydrodynamic damping forces caused by the surrounding fluid, this is a valid assumption for marine vehicles. Combining (22) and (1e), we end up with the sway dynamics

$$\dot{v}_b = \frac{U_b^2}{U_b^2 + X(u_b)u_b}\left(X(u_b)r_\chi + Y(u_b)v_b\right), \tag{32}$$

which will appear in the following analysis.

Lemma 2. *Consider a vehicle described by* (1)*, controlled by the surge and yaw controllers* (21)*. Let Assumption 3-5 hold. Suppose that the course rate, r_χ, is dependent on the sway speed, v_b, in a way that the following holds:*

$$|r_\chi(v_{b,\max})| \leq \frac{|Y_{ud}|}{|X_{ud}|}v_{b,\max}, \tag{33}$$

where $v_{b,\max} > 0$ is constant, and $|v_b(t_0)| \leq v_{b,\max}$. Then,

$$|v_b(t)| \leq v_{b,\max},\ \forall t \geq t_0. \tag{34}$$

Proof: The proof of this lemma follows along the lines of the proof presented in [10, Lemma 2] for the CAA algorithm. Consider the Lyapunov function candidate:

$$V = 0.5v_b^2. \tag{35}$$

Assumption 3 ensures that $u_b(t) = u_{bd},\ \forall t \geq t_0$. The time-derivative of (35) along the trajectories of (32) is then

$$\dot{V} = \frac{U_{bd}^2}{U_{bd}^2 + X_{ud}u_{bd}}\left(X_{ud}r_\chi v_b + Y_{ud}v_b^2\right). \tag{36}$$

By Assumption 4 and 5, (36) satisfies

$$\dot{V} \leq \frac{U_{bd}^2}{U_{bd}^2 + X_{ud}u_{bd}}\left(|X_{ud}|\,|r_\chi|\,|v_b| - |Y_{ud}|\,v_b^2\right). \tag{37}$$

Define the level set $\Omega_v = \{\, v_b \in \mathbb{R} \mid V \leq 0.5v_{b,\max}^2 \,\}$. By (33) and (37), Ω_v is a positively invariant set. Thus, any trajectory starting inside of the set cannot leave it. ∎

Assumption 6. The course rate, r_χ, is bounded by

$$r_\chi \in [-r_{\chi,\max},\, r_{\chi,\max}], \tag{38}$$

where $r_{\chi,\max} > 0$ is a constant parameter.

Remark 5. The maximum course rate is not a physical constraint, rather, it represents a design parameter, similar to $v_{b,\max}$. In the remainder of the analysis, these parameters will be used to reach a set of safety conditions ensuring collision avoidance for the vehicle by the proposed algorithm.

Lemma 3. *Consider a vehicle described by* (1) *and an obstacle described by* (2)*. Let Assumption 1-6 hold, and suppose that $u_b(t) = u_{bd}$ and $|v_b(t)| \leq v_{b,\max}$ for all $t \geq t_0$. Furthermore, suppose that there exists a constant parameter $\sigma \in (0,1)$ such that*

$$v_{b,\max} \leq \sigma\frac{\left(u_{bd}^2 + X_{ud}u_{bd}\right)\sqrt{u_{bd}^2 - u_{o,\max}^2}}{|X_{ud}|\,u_{o,\max}} \tag{39}$$

and

$$r_{\chi,\max} \geq \frac{r_{o,\max}\frac{u_{o,\max}}{u_{bd}} + \frac{a_{o,\max}}{\sqrt{u_{bd}^2 - u_{o,\max}^2}} + \sigma\frac{|Y_{ud}|}{|X_{ud}|}v_{b,\max}}{(1-\sigma)}. \tag{40}$$

Finally, suppose that, at a time $t_1 \geq t_0$, the vehicle satisfies

$$|\chi_{bo}^n(t_1) - \alpha(t_1)| \geq \beta(t_1) \tag{41}$$

and $d_{b,o}(t_1) \geq d_{\text{sep}}$. Then, a course rate, r_χ, satisfying the collision avoidance law (20)*, will keep the vehicle out of conflict for all $t \geq t_1$. Moreover,*

$$d_{b,o}(t) \geq d_{\text{sep}},\ \forall t \geq t_1. \tag{42}$$

Proof: The proof of this lemma follows the same line of arguments as in [5, Theorem 1], where we consider collision avoidance for vehicles with unicycle-type kinematics. We here extend the proof by including the dynamical model of an underactuated surface vehicle, resulting in less flexibility in the choice of $r_{\chi,\max}$ due to the increased model complexity as well as having unactuated dynamics to account for.

Consider the distances to conflict, $\delta^\pm$, defined in (13). By (41), $\delta^{\min}(t_1) \geq 0$. The time-derivative of $\delta^\pm$ is computed by substituting (7) and (10) into (13) as

$$\dot{\delta}^\pm = \pm r_\chi \mp \left(\dot{\alpha} \pm \dot{\beta}\right) \mp \dot{\gamma}_b^\pm. \tag{43}$$

The time-derivative of $\gamma_b^\pm$ is computed from (11) as

$$\dot{\gamma}_b^\pm = \left(-r_o + \dot{\alpha} \pm \dot{\beta}\right)P\left(\gamma_o^\pm\right) + a_o Q\left(\gamma_o^\pm\right) - \dot{v}_b v_b R\left(\gamma_o^\pm\right), \tag{44}$$

where the expressions of $P\left(\gamma_o^\pm\right)$, $Q\left(\gamma_o^\pm\right)$, and $R\left(\gamma_o^\pm\right)$ are given in Appendix A, which yields

$$\begin{aligned}\dot{\delta}^\pm = {} & \pm r_\chi \pm r_o P\left(\gamma_o^\pm\right) \mp a_o Q\left(\gamma_o^\pm\right) \\ & \pm \dot{v}_b v_b R\left(\gamma_o^\pm\right) + \left(1 + P\left(\gamma_o^\pm\right)\right)\left(\mp\dot{\alpha} - \dot{\beta}\right).\end{aligned} \tag{45}$$

The term $\mp\dot{\alpha} - \dot{\beta}$ is computed as

$$\frac{U_{bo}}{d_{b,o}}\left(\pm\sin(\chi_{bo}^n - \alpha) - \cos(\chi_{bo}^n - \alpha)\tan(\beta)\right), \tag{46}$$

where $\dot{\alpha}$ is found geometrically and $\dot{\beta}$ is computed from (8). Recalling that the shortest distance to a conflict, $\delta^{\min}$,

Dette er en postprint-versjon/This is a postprint version.
DOI til publisert versjon/DOI to published version: 10.1109/CCTA48906.2021.9659043

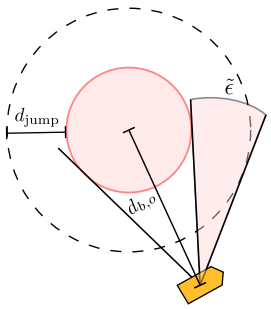

Fig. 3: Geometric representation of $\tilde{\epsilon}$.

satisfies (14), we may write $\pm\sin(\chi_{bo}^n-\alpha) = |\sin(\chi_{bo}^n-\alpha)|$. Furthermore, the vehicle satisfies (41), which entails that

$$|\sin(\chi_{bo}^n-\alpha)| - \cos(\chi_{bo}^n-\alpha)\tan(\beta) \geq 0. \tag{47}$$

Finally, $P\left(\gamma_o^{\pm}\right) \in (-1,1)$ by Assumption 2, thus

$$\begin{aligned}\dot{\delta}^{\pm} \geq \pm r_\chi \left(1 + \frac{X_{ud}v_b U_{bd}^2 R\left(\gamma_o^{\pm}\right)}{U_{bd}^2 + X_{ud}u_{bd}}\right) \pm r_o P\left(\gamma_o^{\pm}\right) \\ \mp a_o Q\left(\gamma_o^{\pm}\right) \pm Y_{ud}v_b^2\left(\frac{U_{bd}^2 R\left(\gamma_o^{\pm}\right)}{U_{bd}^2 + X_{ud}u_{bd}}\right),\end{aligned} \tag{48}$$

where we have inserted the full expression for the sway dynamics given by (32). Consider the term in front of r_χ,

$$\begin{aligned}&1 + \frac{X_{ud}v_b U_{bd}^2 R\left(\gamma_o^{\pm}\right)}{U_{bd}^2 + X_{ud}u_{bd}} \\ \geq &1 - \frac{|X_{ud}||v_b|\,|u_o|}{\left(u_{bd}^2 + X_{ud}u_{bd}\right)\sqrt{u_{bd}^2 - u_o^2}}.\end{aligned} \tag{49}$$

To ensure that (49) is positive, we require $v_{b,\max}$ to satisfy (39), which gives the final expression:

$$\dot{\delta}^{\pm} \geq \pm r_\chi(1-\sigma) \pm r_o P\left(\gamma_o^{\pm}\right) \mp a_o Q\left(\gamma_o^{\pm}\right) - \sigma|v_b|\frac{|Y_{ud}|}{|X_{ud}|}. \tag{50}$$

The remaining terms of (50) are bounded by the conditions of the lemma and Assumption 1 and 2. Thus, if $\delta^{\min} \in [0,\, \epsilon]$, then $\dot{\delta}^{\min} \geq 0$ when r_χ satisfies the collision avoidance law (20) and (40) holds. Hence, by (41), $|\chi_{bo}^n(t) - \alpha(t)| \geq \beta(t),\ \forall t \geq t_1$, which ensures that (42) holds by Lemma 1. ■

The main result will now be presented, where obstacle avoidance is considered in combination with path following. Before stating the theorem, we make the final assumption:

Assumption 7. The vehicle dynamics (1) satisfy

$$\frac{X_{ud}^2 u_{o,\max}\left(r_{o,\max}\frac{u_{o,\max}}{u_{bd}} + \frac{a_{o,\max}}{\sqrt{u_{bd}^2 - u_{o,\max}^2}}\right)}{|Y_{ud}|\left(u_{bd}^2 + X_{ud}u_{bd}\right)\sqrt{u_{bd}^2 - u_{o,\max}^2}} \leq \frac{1}{8}. \tag{51}$$

Remark 6. Assumption 7 follows from Lemma 2 and 3 and ensures that condition (39) and (40) in combination with (33) can be satisfied by a parameter $\sigma \in (0,\, 1)$.

Theorem 1. *Consider a vehicle described by* (1) *and an obstacle described by* (2)*. Let Assumption 1-7 hold, the safety radius satisfy*

$$R_{\text{safe}} \geq d_{\text{sep}} + \frac{U_{bd,\max} + \pi u_{o,\max}}{r_{\chi,\max}} + d_{\text{jump}}, \tag{52}$$

the angular safety distance satisfy

$$\epsilon \geq \arccos\left(\frac{d_{\text{sep}}}{d_{\text{sep}} + d_{\text{jump}}}\right), \tag{53}$$

and the smoothing time satisfy $T_{\text{s}} \leq T_{\text{jump}}$*, where* $d_{\text{jump}} \triangleq T_{\text{jump}}(u_{o,\max} + U_{bd,\max})$ *and* $U_{bd,\max} \triangleq \sqrt{u_{bd}^2 + v_{b,\max}^2}$*. Furthermore, for a constant parameter* $\sigma \in (0,1)$*, let* (39) *and* (40) *of Lemma 3 hold, the maximum course rate satisfy*

$$r_{\chi,\max} \leq \frac{|Y_{ud}|}{|X_{ud}|}v_{b,\max}, \tag{54}$$

and the lookahead distance satisfy

$$\Delta \geq \frac{U_{bd,\max}}{r_{\chi,\max} - \lambda_\chi \pi}. \tag{55}$$

Then, if $d_{b,o}(t_0) \geq R_{\text{safe}}$ *and* $|v_b(t_0)| \leq v_{b,\max}$*, the vehicle controlled by the surge and yaw controllers* (21)*, the guidance system* (15)-(16)*, and the collision avoidance algorithm* (17)-(20)*, will converge to the path* $\mathcal{P}$ *without collision, i.e.* $d_{b,o}(t) \geq d_{\text{sep}},\ \forall t \geq t_0$.

Proof: We will prove this theorem by demonstrating that the lower bounds on the safety radius (52) and the safety angle (53) ensure that the vehicle is able to both reach a safe course and follow the collision avoidance law before a collision can possibly occur with the obstacle.

Lemma 2 in combination with Assumption 6 and the upper bound (54) entails that $|v_b(t)| \leq v_{b,\max},\ \forall t \geq t_0$. The speed of the vehicle is hence bounded by $U_b \leq U_{bd,\max}$.

Consider a time $t_1 \geq t_0$ at which the vehicle and the obstacle are in a conflict, i.e. $\delta^{\min}(t_1) < 0$, and will collide unless the vehicle changes its course. Let also the distance satisfy $d_{b,o}(t_1) = R_{\text{safe}}$. We furthermore consider the worst case scenario in such a situation. A jump in the yaw reference signal occurs at the time t_1, and the time it takes to smooth the signal is upper bounded by T_{jump}, which causes the distance between the vehicle and the obstacle to reduce by d_{jump}. The vehicle must then have reached the maximum course rate, $r_{\chi,\max}$, by (25) and turns at this rate for a full π rad turn before reaching a safe course, during which the obstacle moves at maximum speed towards the turning circle of the vehicle. It follows that the safety radius (52) ensures that there exists a time $t_2 > t_1$ such that $d_{b,o}(t) \geq d_{\text{sep}}, \forall t \in [t_1, t_2]$ and $\delta^{\min}(t_2) = 0$. Lemma 3 then ensures that $d_{b,o} \geq d_{\text{sep}}$ until guidance resumes.

Suppose now that, at some time $t_3 > t_0$, the guidance law satisfies $\chi_{\text{gd}}^n \in \mathcal{V}_{\text{cc}}^{\epsilon}$ during which $d_{b,o} < R_{\text{safe}}$, causing the collision avoidance scheme to commence. The vehicle is not guaranteed to follow (20) before the time T_{jump} has passed. By (18), there must exist a time $t_3' < t_3$ such that $d_{b,o}(t_3') \geq \frac{d_{\text{sep}}}{\cos(\epsilon)}$ and $\chi_b^n(t) \notin \mathcal{V}_{\text{cc}}^{\epsilon}, \forall t \in [t_3', t_3]$, which entails by Lemma 1 and the choice of ϵ in (53) that

$$d_{b,o}(t_3) \geq \frac{d_{\text{sep}}}{\cos(\epsilon)} \geq d_{\text{sep}} + d_{\text{jump}}. \tag{56}$$

Dette er en postprint-versjon/This is a postprint version.
DOI til publisert versjon/DOI to published version: 10.1109/CCTA48906.2021.9659043

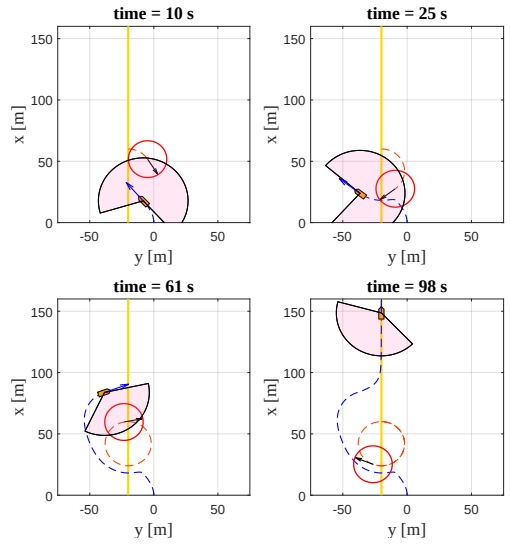

Fig. 4: The first simulation. The distance d_{sep} from the obstacle center is represented by the red circle and the vehicle by the orange polygon. The obstacle and vehicle trajectories are shown as the red and blue dashed lines, respectively. The path, $\mathcal{P}$, is given by the yellow line and χ_b^n by the blue vector. The domain $\mathcal{V}_{\text{cc}}^{\epsilon}$ is shown as the red, transparent sector, with a radius of R_{safe}.

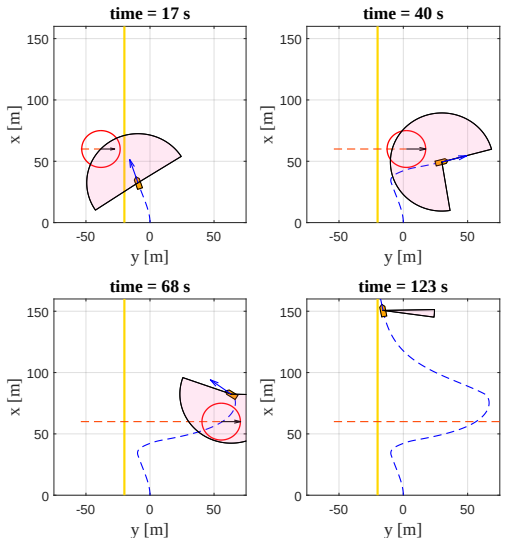

Fig. 5: The second simulation.

Furthermore, consider Figure 3 which illustrates the worst case reduction of $\delta^{\min}$ during the time T_{jump}, given by

$$\tilde{\epsilon} \triangleq \arccos\left(\frac{d_{\text{sep}}}{d_{\text{sep}} + d_{\text{jump}}}\right). \tag{57}$$

It follows that the safety angle (53) ensures that $d_{b,o}(t) \geq d_{\text{sep}}$, $\delta^{\min}(t) \geq 0$, $\forall t \in [t_3, t_3 + T_{\text{jump}}]$. Lemma 3 ensures that a collision does not occur thereafter.

Finally, since $u_b > u_{o,\max}$, the vehicle will eventually escape the obstacle and resume path following, during which the vehicle cannot enter a collision by Lemma 1 and the safety criteria (17) and (18). The choice of Δ in (55) entails that $|r_{\text{gd}}| \leq r_{\chi,\max}$, ensuring that χ_{gd}^n will be perfectly followed. When tracked, the LOS guidance law (15) provides uniform semiglobal exponential convergence of the cross-track error $e \triangleq y_b^n - y_{\text{t}}^n$ to zero [11], concluding the proof. ■

VII. Simulation Results

This section presents two numerical simulations of the underactuated surface vehicle (1), governed by the control system presented in Section V. The model parameters belong to an LAUV [14], operating in three degrees of freedom. In both simulations, the desired surge speed of the vehicle is chosen as $u_{bd} = 2$ m/s, the initial heading as $\psi_b^n(t_0) = 0$ rad, and the initial position as $\boldsymbol{p}_b^n(t_0) = [0,\ 0]^\top$ m. Assumption 4 and 5 hold with $Y(u_{bd}) = -2.8161$ and $X(u_{bd}) = -1.0242$. We choose the control gains as $\lambda_\chi = 0.1$ and $\lambda_\delta = \lambda_r = \lambda_u = 1$. The obstacle (2) has a radius of $R_o = 10$ m. The separation distance is chosen as $d_{\text{sep}} = 15$ m and the desired y^n-position as $y_{\text{t}}^n = -20$ m.

In the first scenario, the obstacle turns in a clockwise circle at a constant speed of $u_o = u_{o,\max} = 1.8$ m/s and turning rate of $r_o = r_{o,\max} = 0.1$ rad/s. We choose $\sigma = 0.3$, $v_{b,\max} = 0.27$ m/s, and $r_{\chi,\max} = 0.74$ rad/s, according to Theorem 1. The smoothing time is upper bounded by $T_{\text{jump}} = 2.33$ s. The safety radius is chosen as $R_{\text{safe}} = 35$ m, the safety angle as $\epsilon = 0.9$ rad, and the lookahead distance as $\Delta = 5$ m, satisfying the conditions of Theorem 1.

The trajectories of the vehicle and the obstacle are plotted in Figure 4 at four different times. At $t = 10$ s, the distance is reduced to $d_{b,o} = R_{\text{safe}}$ simultaneously as $\delta^{\min} < 0$. The collision avoidance scheme is then initiated, which makes the vehicle turn left at the maximum rate. The vehicle obtains a safe course before a collision occurs, which is maintained throughout the maneuver. Once the vehicle has circumvented the obstacle by following the collision avoidance law (20), the guidance course satisfies (18), causing the vehicle to resume path following. The vehicle has converged to the path at $t = 98$ s without collision. The distance to the obstacle, $d_{b,o}$, and the sway speed of the vehicle, v_b, during the simulation is shown in the left-most plots of Figure 6, thus supporting the theoretical result of Theorem 1.

In the second scenario, the obstacle approaches the vehicle from the left at a constant acceleration of $a_o = a_{o,\max} = 0.05$ m/s^2 and zero turning rate. The initial speed of the obstacle is $u_o(t_0) = 0.5$ m/s, and its maximum speed is $u_{o,\max} = 1.9$ m/s. The control parameters are respectively $\sigma = 0.25$, $v_{b,\max} = 0.15$ m/s, $r_{\chi,\max} = 0.41$ rad/s, $T_{\text{jump}} = 1.28$ s, $R_{\text{safe}} = 40$ m, $\epsilon = 0.73$ rad, and $\Delta = 21$ m, chosen to satisfy the conditions of Theorem 1.

The trajectories of the vehicle and the obstacle are plotted in Figure 5. The vehicle is approaching the path as the distance to the obstacle is reduced to R_{safe}. The vehicle turns right in accordance with (19) to avoid a collision. As the vehicle attempts to avoid the obstacle by moving to the right, the obstacle accelerates directly towards it. Despite this, the vehicle is able to maintain at least the distance d_{sep} to the obstacle at all times, during which the sway speed remains within the upper bound $v_{b,\max}$, as verified by the right-most plots of Figure 6. The vehicle escapes the obstacle at $t = 68$ s and converges to the path. Hence, the simulation results confirm the theoretical result of Theorem 1.

Dette er en postprint-versjon/This is a postprint version.
DOI til publisert versjon/DOI to published version: 10.1109/CCTA48906.2021.9659043

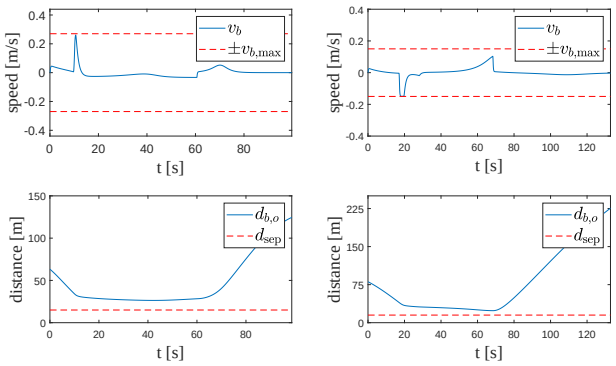

Fig. 6: Distance, $d_{b,o}$, and sway speed, v_b, during the first and second simulation, given in the left and right plots, respectively.

VIII. Conclusions and Future Work

In this paper, we have proposed and analyzed a reactive collision avoidance algorithm, applied to a surface vehicle that lacks actuation in the sideways direction. Rather than neglecting the unactuated dynamics of the vehicle, we specifically considered the sway dynamics in the control design and analysis of the system. The proposed collision avoidance law is based on the concept of a conflict, a condition implying that the vehicle is headed towards a collision with an obstacle. By making the vehicle stay out of conflicts, we ensure that the vehicle avoids a collision. To achieve this for an underactuated vehicle encountering a dynamic obstacle, we considered the dynamic capabilities and constraints of both the vehicle and the obstacle in the design of our approach. Furthermore, we showed that collision avoidance was guaranteed in any scenario, under explicit conditions derived by our analysis of the complete, closed-loop system. The collision avoidance problem was combined with path following to demonstrate that other goal-reaching behaviour of the vehicle is easily incorporated into the algorithm due to its modular structure. Simulations of an underactuated marine vehicle moving in three degrees of freedom were included to verify the theoretical analysis.

Future work concerns the issue of avoiding multiple moving obstacles, as well as obstacles of arbitrary shape.

Appendix

A. Functional expressions

The functional expressions of the model (1) are defined:

$$f_u(u_b, v_b, r_b) \triangleq r_b \frac{r_b m_{23} + v_b m_{22}}{m_{11}} - u_b \frac{d_{11}}{m_{11}}, \tag{58}$$

$$f_r(u_b, v_b, r_b) \triangleq r_b \frac{m_{23}\left(d_{23} - m_{11}u_b\right) - m_{22}\left(d_{33} + m_{23}u_b\right)}{m_{22}m_{33} - m_{23}^2} + v_b \frac{m_{23}d_{22} + m_{22}\left(d_{32} + u_b\left(m_{22} - m_{11}\right)\right)}{m_{22}m_{33} - m_{23}^2}, \tag{59}$$

$$X(u_b) \triangleq \frac{d_{33}m_{23} - d_{23}m_{33} + u_b\left(m_{23}^2 - m_{11}m_{33}\right)}{m_{22}m_{33} - m_{23}^2}, \tag{60}$$

$$Y(u_b) \triangleq \frac{d_{32}m_{23} - d_{22}m_{33} + u_b m_{23}\left(m_{22} - m_{11}\right)}{m_{22}m_{33} - m_{23}^2}, \tag{61}$$

where m_{ij} and d_{ij} are the elements of the inertia- and damping matrix (including added mass) [12].

The expressions derived in Lemma 3 are defined:

$$P(\gamma_o) \triangleq \frac{u_o \cos(\gamma_o)}{U_{\text{bd}}\sqrt{1 - \left(u_o/U_{\text{bd}}\right)^2 \sin^2(\gamma_o)}}, \tag{62a}$$

$$Q(\gamma_o) \triangleq \frac{\sin(\gamma_o)}{U_{\text{bd}}\sqrt{1 - \left(u_o/U_{\text{bd}}\right)^2 \sin^2(\gamma_o)}}, \tag{62b}$$

$$R(\gamma_o) \triangleq \frac{u_o \sin(\gamma_o)}{U_{\text{bd}}^3\sqrt{1 - \left(u_o/U_{\text{bd}}\right)^2 \sin^2(\gamma_o)}}. \tag{62c}$$

Acknowledgment

This work was supported by the Research Council of Norway through the Centres of Excellence funding scheme, project No. 223254 – NTNU AMOS.

References

[1] P. Fiorini and Z. Shiller, "Motion planning in dynamic environments using velocity obstacles," *The International Journal of Robotics Research*, vol. 17, no. 7, pp. 760–772, 1998.

[2] A. Chakravarthy and D. Ghose, "Obstacle avoidance in a dynamic environment: a collision cone approach," *IEEE Transactions on Systems, Man, and Cybernetics - Part A: Systems and Humans*, vol. 28, no. 5, pp. 562–574, 1998.

[3] V. Sunkara, A. Chakravarthy, X. Yi, W. Zuo, and Z. Chen, "Cooperative optimal collision avoidance laws for a hybrid-tailed robotic fish," *IEEE Transactions on Control Systems Technology*, vol. 28, no. 4, pp. 1569–1578, 2020.

[4] V. Sunkara and A. Chakravarthy, "Collision avoidance laws for objects with arbitrary shapes," in *2016 IEEE 55th Conference on Decision and Control (CDC)*, pp. 5158–5164, 2016.

[5] A. Haraldsen, M. S. Wiig, and K. Y. Pettersen, "Vehicle safety of the velocity obstacle algorithm," in *2020 59th IEEE Conference on Decision and Control (CDC)*, pp. 5340–5347, 2020.

[6] J. Alonso-Mora, T. Naegeli, R. Siegwart, and P. Beardsley, "Collision avoidance for aerial vehicles in multi-agent scenarios," *Autonomous Robots*, vol. 39, no. 1, pp. 101–121, 2015.

[7] W. Zhang, S. Wei, Y. Teng, J. Zhang, X. Wang, and Z. Yan, "Dynamic obstacle avoidance for unmanned underwater vehicles based on an improved velocity obstacle method," *Sensors*, vol. 17, no. 12, p. 2742, 2017.

[8] Y. Cho, J. Han, J. Kim, P. Lee, and S.-B. Park, "Experimental validation of a velocity obstacle based collision avoidance algorithm for unmanned surface vehicles," *IFAC-PapersOnLine*, vol. 52, no. 21, pp. 329–334, 2019. IFAC Conference on Control Applications in Marine Systems, Robotics, and Vehicles.

[9] Y. Huang, L. Chen, and P. Gelder, "Generalized velocity obstacle algorithm for preventing ship collisions at sea," *Ocean Engineering*, vol. 173, pp. 142–156, 2019.

[10] M. S. Wiig, K. Y. Pettersen, and T. R. Krogstad, "Collision avoidance for underactuated marine vehicles using the constant avoidance angle algorithm," *IEEE Transactions on Control Systems Technology*, vol. 28, no. 3, pp. 951–966, 2020.

[11] T. I. Fossen and K. Y. Pettersen, "On uniform semiglobal exponential stability (USGES) of proportional line-of-sight guidance laws," *Automatica*, vol. 50, no. 11, pp. 2912–2917, 2014.

[12] T. I. Fossen, *Handbook of Marine Craft Hydrodynamics and Motion Control*. John Wiley & Sons, 2011.

[13] E. Lalish, K. A. Morgansen, and T. Tsukamaki, "Decentralized reactive collision avoidance for multiple unicycle-type vehicles," in *American Control Conference*, pp. 5055–5061, 2008.

[14] J. Estrela da Silva, B. Terra, R. Martins, and J. Sousa, "Modeling and simulation of the LAUV autonomous underwater vehicle," in *IEEE IFAC International Conference on Methods and Models in Automation and Robotics*, 2007.

Dette er en postprint-versjon/This is a postprint version.
DOI til publisert versjon/DOI to published version: 10.1109/CCTA48906.2021.9659043